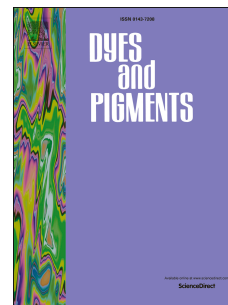


Accepted Manuscript

Mechanofluorochromism of NIR-emitting dyes based on difluoroboron β -carbonyl cyclic ketonate complexes

Fushuang Zhang, Lu Zhai, Siwei Feng, Wenhua Mi, Jingbo Sun, Meng Sun, Jinyu Zhao, Ran Lu



PII: S0143-7208(18)30315-2

DOI: [10.1016/j.dyepig.2018.03.069](https://doi.org/10.1016/j.dyepig.2018.03.069)

Reference: DYPI 6654

To appear in: *Dyes and Pigments*

Received Date: 11 February 2018

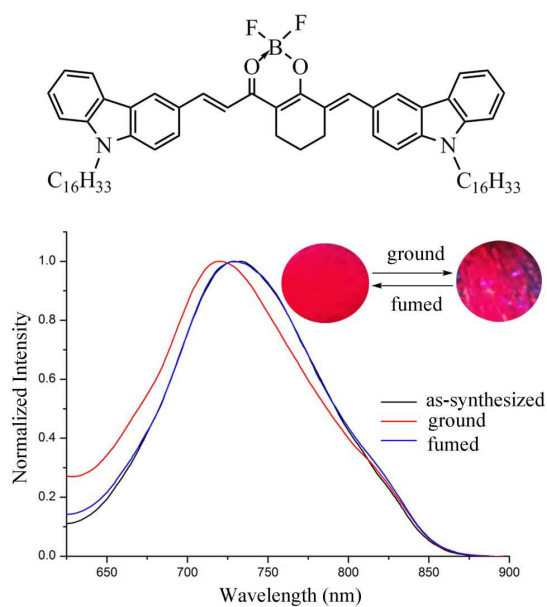
Revised Date: 27 March 2018

Accepted Date: 28 March 2018

Please cite this article as: Zhang F, Zhai L, Feng S, Mi W, Sun J, Sun M, Zhao J, Lu R, Mechanofluorochromism of NIR-emitting dyes based on difluoroboron β -carbonyl cyclic ketonate complexes, *Dyes and Pigments* (2018), doi: 10.1016/j.dyepig.2018.03.069.

This is a PDF file of an unedited manuscript that has been accepted for publication. As a service to our customers we are providing this early version of the manuscript. The manuscript will undergo copyediting, typesetting, and review of the resulting proof before it is published in its final form. Please note that during the production process errors may be discovered which could affect the content, and all legal disclaimers that apply to the journal pertain.

Mechanofluorochromism of NIR-emitting dyes based on difluoroboron β -carbonyl cyclic ketonate complexes



Mechanofluorochromism of NIR-emitting dyes based on difluoroboron β -carbonyl cyclic ketonate complexes

Fushuang Zhang,^a Lu Zhai,^a Siwei Feng,^b Wenhua Mi,^a Jingbo Sun,^a Meng Sun,^a Jinyu Zhao^a and Ran Lu^{*,a}

^a State Key Laboratory of Supramolecular Structure and Materials, College of Chemistry, Jilin University, Changchun 130012, P. R. China

^b College of Life Sciences, Jilin University, Changchun 130021, P. R. China

Abstract

New difluoroboron β -carbonyl cyclic ketonate complexes **CnB** ($n = 2, 16$), in which carbazole was linked to difluoroboron β -diketonate directly, and **DCnB** ($n = 2, 16$), where two terminal carbazole units were bridged by vinyl groups to link to difluoroboron β -diketonate core, were synthesized. They exhibited reversible mechanofluorochromic (MFC) behavior under grinding/fuming or heating treatment. Particularly, the emission of **DC2B** and **DC16B** emerged in the range of 650-850 nm in the solid-state. They gave red and rose-red luminescence in the as-synthesized crystals and in ground powders, respectively, during MFC processes. Such MFC materials emitting NIR (near-infrared) light were seldom reported. In addition, compared with **C2B**, **C16B** showed high-contrast mechanofluorochromism because the long alkyl chain might decrease the strength of π - π interactions in the as-synthesized crystals, leading to the emission appeared at the high-energy region (483 nm). The disassembling of parts of π -aggregates and the improvement of the molecular planarity led to relative obvious red-shift of the emission (509 nm) upon grinding.

Keywords: difluoroboron β -diketonate, carbazole, mechanofluorochromism, NIR emission

ACCEPTED MANUSCRIPT

* Corresponding author. State Key Laboratory of Supramolecular Structure and Materials, College of Chemistry, Jilin University, Changchun 130012, P. R. China
E-mail: luran@mail.jlu.edu.cn

1. Introduction

As one kind of stimuli-responsive luminescent organic materials, mechanofluorochromic (MFC) dyes have received much attention on account of their potential applications in sensors, memory chips, data storage and security inks.¹⁻² Generally, the emitting colors of MFC compounds can be altered induced by external forces of stretching, grinding, pressing and shearing.³⁻⁴ It has been known that the changes in the molecular packing or/and molecular conformation driven by mechanical forces are responsible for the MFC behavior, and the mechanofluorochromism is often reversible.⁵⁻⁷ However, the design of MFC dyes is still challenging because the aggregation-caused quenching (ACQ) often results in the decrease of the emission intensity in the solid-state.⁵ Solid-state NIR-emitting dyes were seldom reported since the molecules with low-lying excited states often contain extended conjugated systems or donor/acceptor moieties, which would lead to strong π - π interactions as well as ACQ effect.⁸ It should be noted that the difluoroboron β -diketonate (BF₂bdk) complexes are attractive fluorophores,⁹ and a number of MFC materials based on BF₂bdk have been documented to date. Fraser and co-workers found that the solid-state emission of difluoroboron β -diketonate complexes bearing arenes changed upon the stimulation of mechanical forces.⁶ Šket *et al.* synthesized the difluoroboron complex of 1-phenyl-3-(3,5-dimethoxyphenyl)-propane-1,3-dione, and two kinds of polymorphs were obtained. By controllable alteration of the molecular arrangements through external forces, varying solid-state emission was achieved from the same dye.¹⁰ Liu *et al.* revealed that the force induced formation of emissive *H*-aggregates and energy transfer to *H*-aggregates were responsible for the mechanofluorochromism of difluoroboron dibenzoylmethane in the solid-state.¹¹ Our group previously reported that some D- π -A type difluoroboron β -diketonate

complexes with ICT emission exhibited MFC behavior.¹² Up to data, limited studies focused on MFC materials with NIR emission,¹³ which may have promising applications in bioimaging¹⁴ and security inks.¹⁵ Moreover, the length of the alkyl chains were found to be another factor to affect the MFC properties.¹⁶ With these in mind, we synthesized new carbazole modified difluoroboron β -carbonyl cyclic ketonate complexes **CnB** and **DCnB** ($n = 2, 16$, Scheme 1), which exhibited reversible MFC behavior.

2. Experimental Section.

2.1. Materials and methods

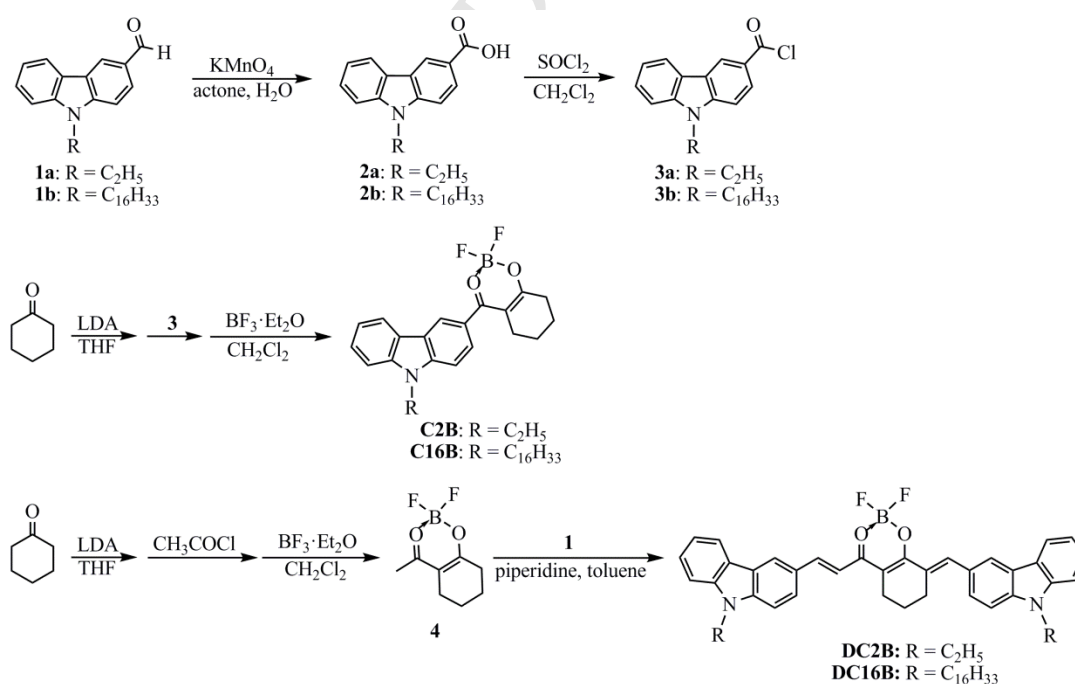
¹H NMR and ¹³C NMR spectra were measured using a Mercury Plus instrument at 400 MHz and 101 MHz using CDCl₃ and DMSO-*d*₆ as solvent. FT-IR spectra were measured using a Nicolet-360 FT-IR spectrometer by incorporation of samples in KBr disks. The UV-vis absorption spectra were obtained on a Shimadzu UV-3100 spectrophotometer. Fluorescent emission spectra were obtained on a Cary Eclipse fluorescence spectrophotometer. Mass spectra were obtained with Agilent 1100 MS series and AXIMA CFR MALDI-TOF (Compact) mass spectrometers. C, H, and N elemental analyses were taken on a Vario EL cube elemental analyzer. XRD patterns were obtained on an Empyrean X-ray diffraction instrument. The single crystal of **C2B** was obtained in 1,4-dioxane and *n*-hexane *via* solvent diffusion, and selected for X-ray diffraction analysis on a Rigaku RA XIS-RA PID diffractometer using graphite-monochromated MoK α radiation ($\lambda = 0.71073 \text{ \AA}$). The crystal was kept at room temperature during data collection. Differential scanning calorimetry (DSC) curves were obtained on a Netzsch DSC 204F1 at a heating rate of 10 °C/min.

THF and toluene were dried over sodium and benzophenone under nitrogen. CH_2Cl_2 was dried over calcium hydride. The other chemicals and reagents were used as received without further purification. Compounds **1** and **2** were prepared according to the reported procedures.¹⁷

2.2. Synthesis

9-Ethyl-9H-carbazole-3-carbonyl chloride (**3a**)^{12b}

The solution of 9-ethyl-9H-carbazole-3-carboxylic acid (**2a**, 1.0 g, 4.2 mmol) in CH_2Cl_2 (10.0 mL) was cooled at 0 °C. Then, SOCl_2 (0.5 mL, 4.3 mmol) was added, followed by adding four drops of dry DMF. The mixture was warmed to room temperature and stirred at room temperature for 3 h. It should be noted that the excess SOCl_2 was removed completely under vacuum when the reaction was finished. The residuum of 9-ethyl-9H-carbazole-3-carbonyl chloride (**3a**) was not further purified and used directly in the next step.



Scheme 1 Synthetic routes for **C2B**, **C16B**, **DC2B** and **DC16B**.

9-Hexadecyl-9H-carbazole-3-carbonyl chloride (3b)

Following the synthetic procedure of **3a**, compound **3b** was synthesized from 9-hexadecyl-9H-carbazole-3-carboxylic acid (**2b**, 1.00 g, 2.3 mmol) and SOCl₂ (0.25 mL, 3.5 mmol), and it was used directly in the next step without further purification.

2,2-Difluoro-4-methyl-5,6,7,8-tetrahydro-2H-2λ⁴,3λ³-benzo[d] [1,3,2] dioxaborinine (4)^{12b}

LDA (2 M in THF, 12.70 mL, 25.40 mmol) was added to dry THF (10.0 mL) in 100 mL flask under N₂ atmosphere, and the mixture was cooled to -78 °C. Cyclohexanone (2.7 mL, 25.40 mmol) in dry THF (5.0 mL) was then added dropwise. After stirring at -78 °C for 1 h, acetyl chloride (1.00 g, 12.70 mmol) in dry THF (5.0 mL) was added dropwise. After that, the solution was allowed to warm to room temperature and stirred at room temperature for another 18 h. The mixture was quenched by HCl (2 M), and the crude product was extracted with ethyl acetate (3 × 50 mL). The organic layers were combined and dried with anhydrous MgSO₄. After removal the solvent, a yellow solid, 1-(2-hydroxycyclohex-1-ene-1-yl)ethan-1-one was complexed with boron trifluoride diethyl etherate complex directly. In detail, the crude intermediate was dissolved in dry CH₂Cl₂ (25 mL), and boron trifluoride diethyl ether (3.3 mL, 25.40 mmol) was added. The mixture was refluxed under an atmosphere of nitrogen for 2 h. Excess CH₂Cl₂ was removed under vacuum to give the crude product, which was purified by column chromatography (silica gel, CH₂Cl₂/petroleum ether, v/v = 10/1), followed by recrystallization from the mixed solvent of CH₂Cl₂/petroleum ether to afford **4** (1.42 g) in 59 % yield. m.p. 73.9-74.1 °C. ¹H NMR (400 MHz, CDCl₃) δ 2.58 (t, *J* = 5.9 Hz, 2H), 2.39 (t, *J* = 5.6 Hz, 2H), 2.30 (s, 3H), 1.82-1.75 (m, 4H) (Fig.

S7, ESI[†]). ¹³C NMR (101 MHz, CDCl₃) δ 191.88 (s), 190.01 (s), 108.99 (s), 32.44 (s), 23.13 (s), 22.24 (s), 21.91 (s), 20.89 (s) (Fig. S8, ESI[†]).¹⁸

3-(2,2-Difluoro-5,6,7,8-tetrahydro-2H-2λ⁴,3λ³-benzo[d][1,3,2]dioxaborinin-4-yl)-9-ethyl-9H-carbazole (C2B)

Following the synthetic procedure of **4**, complex **C2B** was synthesized from the ligand (9-ethyl-9H-carbazol-3-yl)(2-hydroxycyclohex-1-en-1-yl)methanone, which was prepared from **3a** (1.00 g, 4.20 mmol), cyclohexanone (0.87 mL, 8.40 mmol) and LDA (4.20 mL, 8.40 mmol) in dry THF, and boron trifluoride diethyl etherate complex (1.1 mL, 8.40 mmol) in dry CH₂Cl₂ (25 mL). The crude product was purified by column chromatography (silica gel, CH₂Cl₂/petroleum ether, v/v = 10/1), followed by recrystallization from the mixed solvent of CH₂Cl₂/petroleum ether to afford **C2B** (0.85 g) in 55 % yield. m.p. 174.5-175.0 °C. ¹H NMR (400 MHz, CDCl₃) δ 8.68 (s, 1H), 8.14 (d, *J* = 7.7 Hz, 1H), 8.01 (d, *J* = 8.7 Hz, 1H), 7.55 (t, *J* = 5,6 Hz, 1H), 7.46 (dd, *J* = 13.2, *J* = 8.5 Hz, 2H), 7.34 (t, *J* = 7.4 Hz, 1H), 4.43-4.38 (m, 2H), 2.81 (t, *J* = 5.8 Hz, 2H), 2.72 (t, *J* = 6.5 Hz, 2H), 1.93-1.87 (m, 2H), 1.75-1.71 (m, 2H), 1.47 (t, *J* = 7.2 Hz, 3H) (Fig. S9, ESI[†]). ¹³C NMR (101 MHz, CDCl₃) δ 189.94 (s), 184.48 (s), 142.88 (s), 140.62 (s), 128.16 (s), 126.93 (s), 124.14 (s), 123.34 (s), 122.87 (d, *J* = 1.8 Hz), 120.81 (s), 120.53 (s), 109.24 (s), 108.25 (d, *J* = 13.5 Hz), 37.94 (s), 32.95 (s), 26.79 (s), 23.11 (s), 21.33 (s), 13.82 (s) (Fig. S10, ESI[†]). MALDI-TOF MS: m/z: calculated for C₂₁H₂₀BF₂N₂O₂: 367.2; found: 365.3 [M-2]⁺ (Fig. S11, ESI[†]); FT-IR (KBr, cm⁻¹): 2925, 2848, 1530, 1473, 1367, 1034, 747. Elem. Anal. Calcd. (%) for C₂₁H₂₀BF₂NO₂: C, 68.69; H, 5.49; N, 3.81. Found: C, 68.38; H, 5.43; N, 3.93.

3-(2,2-Difluoro-5,6,7,8-tetrahydro-2H-2λ⁴,3λ³-benzo[d][1,3,2]dioxaborinin-4-yl)-9-hexadecyl-9H-carbazole (C16B)

Following the synthetic procedure of **4**, complex **C16B** was synthesized from the ligand (9-hexadecyl-9H-carbazol-3-yl)(2-hydroxycyclohex-1-en-1-yl)methanone, which was prepared from **3b** (1.00 g, 2.30 mmol), cyclohexanone (0.48 mL, 4.60 mmol) and LDA (2.30 mL, 4.60 mmol) in dry THF, and boron trifluoride diethyl etherate complex (0.58 mL, 4.60 mmol) in dry CH₂Cl₂ (25 mL). The crude product was purified by column chromatography (silica gel, CH₂Cl₂/petroleum ether, v/v = 10/1), followed by recrystallization from the mixed solvent of CH₂Cl₂/petroleum ether to afford **C16B** (0.80 g) in 62 % yield. m.p. 91.0-91.5 °C. ¹H NMR (400 MHz, CDCl₃) δ 8.69 (s, 1H), 8.15 (d, *J* = 7.7 Hz, 1H), 8.01 (d, *J* = 3.8 Hz, 1H), 7.55 (t, *J* = 7.3 Hz, 1H), 7.45 (t, *J* = 9.6 Hz, 2H), 7.34 (t, *J* = 7.4 Hz, 1H), 4.33 (t, *J* = 7.2 Hz, 2H), 2.82 (t, *J* = 5.9 Hz, 2H), 2.72 (t, *J* = 6.6 Hz, 2H), 1.92-1.85 (m, 4H), 1.77-1.71 (m, 2H), 1.24 (d, *J* = 4.8 Hz, 26H), 0.88 (t, *J* = 6.8 Hz, 3H) (Fig. S12, ESI[†]). ¹³C NMR (101 MHz, CDCl₃) δ 189.91 (s), 184.50 (s), 143.41 (s), 141.11 (s), 128.17 (s), 126.91 (s), 124.14 (s), 123.32 (s), 122.79 (d, *J* = 3.7 Hz), 120.77 (s), 120.52 (s), 109.49 (s), 108.45 (s), 108.31 (s), 43.45 (s), 32.96 (s), 31.94 (s), 29.59 (ddd, *J* = 23.8, 11.2, 6.4 Hz), 28.93 (s), 27.25 (s), 26.83 (s), 23.14 (s), 22.71 (s), 21.36 (s), 14.14 (s) (Fig. S13, ESI[†]). MALDI-TOF MS: m/z: calculated for C₃₅H₄₈BF₂NO₂: 563.6; found: 561.6 [M-2]⁺ (Fig. S14, ESI[†]); FT-IR (KBr, cm⁻¹): 2916, 2849, 1543, 1490, 1474, 1373, 1038, 741. Elem. Anal. Calcd. (%) for C₃₅H₄₈BF₂NO₂: C, 74.59; H, 8.59; N, 2.49. Found: C, 74.35; H, 9.04; N, 2.39.

9-Ethyl-3-((E)-2-((E)-8-((9-ethyl-9H-carbazol-3-yl)methylene)-2,2-difluoro-5,6,7,8-tetrahydro-2H-2λ⁴,3λ³-benzo[d][1,3,2]dioxaborinin-4-yl)vinyl)-9H-carbazole (DC2B)

Compounds **4** (0.63 g, 3.35 mmol) and **1a** (0.75 g, 3.35 mmol) were dissolved in dry toluene (20 mL), and four drops of piperidine were added. The mixture was refluxed for 2 h. Water (80 mL) was added to the cooled solution and the mixture was extracted with CH₂Cl₂ (3 × 50 mL). The organic layers were combined and dried with anhydrous MgSO₄. After removal the solvent, the crude product was purified by column chromatography (silica gel, CH₂Cl₂/petroleum ether, v/v = 10/1), followed by recrystallization from the mixed solvent of CH₂Cl₂/petroleum ether to afford **DC2B** (0.98 g) in 49 % yield. m.p. 278.0-279.0 °C. ¹H NMR (400 MHz, CDCl₃) δ 8.27 (d, *J* = 17.8 Hz, 3H), 8.16-8.10 (m, 3H), 7.71 (d, *J* = 8.6 Hz, 1H), 7.56 (d, *J* = 8.6 Hz, 1H), 7.50 (t, *J* = 7.4 Hz, 2H), 7.39-7.27 (m, 6H), 7.00 (d, *J* = 15.1 Hz, 1H), 4.32-4.25 (m, 4H), 2.90 (t, *J* = 5.5 Hz, 2H), 2.71 (t, *J* = 6.0 Hz, 2H), 1.90-1.84 (m, 2H), 1.44-1.39 (m, 6H) (Fig. S15, ESI[†]). ¹³C NMR (101 MHz, DMSO-*d*₆) δ 176.67 (s), 175.33 (s), 149.13 (s), 142.09 (s), 140.24 (t, *J* = 15.5 Hz), 129.52 (s), 128.46 (s), 128.18 (s), 126.56 (d, *J* = 20.6 Hz), 126.01 (s), 125.60 (s), 124.47 (s), 123.62 (s), 123.03 (s), 122.65 (s), 122.28 (d, *J* = 7.8 Hz), 120.86 (s), 120.06 (s), 119.68 (s), 114.24 (s), 109.93 (s), 109.67-109.26 (m), 54.89 (s), 43.72 (s), 37.33 (s), 26.74 (s), 22.78 (s), 22.18 (s), 21.80 (s), 13.77 (s) (Fig. S16, ESI[†]). MALDI-TOF MS: *m/z*: calculated for C₃₈H₃₃BF₂N₂O₂: 598.5; found: 596.8 [M-2]⁺ (Fig. S17, ESI[†]); FT-IR (KBr, cm⁻¹): 2928, 2847, 1740, 1581, 1473, 1231, 1189, 1108, 1025, 963, 731. Elem. Anal. Calcd. (%) for C₃₈H₃₃BF₂N₂O₂: C, 76.26; H, 5.56; N, 4.68. Found: C, 75.87; H, 5.73; N, 5.05.

3-((E)-(2,2-Difluoro-4-((E)-2-(9-hexadecyl-9H-carbazol-3-yl)vinyl)-6,7-dihydro-2H-2λ⁴,3λ³-benzo[d][1,3,2]dioxaborinin-8(5H)-ylidene)methyl)-9-hexadecyl-9H-carbazole (DC16B)

The synthetic method for **DC16B** was similar to that for **DC2B** except using compounds **4** (1.00 g, 2.4 mmol) and **1b** (0.22 g, 2.4 mmol) as reactants. The crude product was purified by column chromatography (silica gel, CH₂Cl₂/petroleum ether, v/v = 10/1), followed by recrystallization from the mixed solvent of CH₂Cl₂/petroleum ether to afford **DC16B** (1.00 g) in 42 % yield. m.p. 152.3-153.9 °C. ¹H NMR (400 MHz, CDCl₃) δ 8.31 (d, *J* = 17.9 Hz, 3H), 8.21 (s, 1H), 8.13 (dd *J* = 11.6, 7.7 Hz, 2H), 7.73 (d, *J* = 7.5 Hz, 1H), 7.59 (d, *J* = 8.1 Hz, 1H), 7.50 (t, *J* = 7.4 Hz, 2H), 7.38 (t, *J* = 8.2 Hz, 4H), 7.30 (dd, *J* = 15.7, 7.9 Hz, 2H), 7.04 (d, *J* = 15.1 Hz, 1H), 4.23 (dd, *J* = 13.5, 6.8 Hz, 4H), 2.95 (t, *J* = 5.2 Hz, 2H), 2.76 (t, *J* = 6.0 Hz, 2H), 1.92-1.84 (m, 6H), 1.24 (d, *J* = 5.1 Hz, 52H), 0.88 (t, *J* = 6.8 Hz, 6H) (Fig. S18, ESI[†]). ¹³C NMR (101 MHz, CDCl₃) δ 176.66 (s), 176.30 (s), 148.86 (s), 142.60 (s), 141.33 (s), 140.91 (t, *J* = 26 Hz), 129.67 (s), 127.90 (s), 127.29 (s), 126.44 (s), 126.22 (s), 125.70 (s), 123.90 (s), 123.55 (s), 123.04 (s), 122.80 (d, *J* = 4.6 Hz), 120.70 (d, *J* = 52 Hz), 120.09 (s), 119.72 (s), 113.70 (s), 109.25 (d, *J* = 8 Hz), 109.05 (s), 108.63 (d, *J* = 16 Hz), 99.98 (s), 43.15 (s), 31.95 (s), 29.82–29.46 (m), 29.36 (d, *J* = 16 Hz), 28.92 (d, *J* = 20 Hz), 27.25 (d, *J* = 16 Hz), 27.04 (s), 23.45 (s), 22.71 (s), 22.20 (s), 14.15 (s) (Fig. S19, ESI[†]). MALDI-TOF MS: *m/z*: calculated for C₆₆H₈₉BF₂NO₂: 991.2; found: 989.2 [M-2]⁺ (Fig. S20, ESI[†]); FT-IR (KBr, cm⁻¹): 2920, 2850, 1248, 1740, 1581, 1749, 1255, 1193, 1112, 1029, 967, 728. Elem. Anal. Calcd. (%) for C₆₆H₈₉BF₂N₂O₂: C, 79.97; H, 9.05; N, 2.83. Found: C, 79.59; H, 9.31; N, 3.17.

3. Results and Discussion

3.1. Synthesis

The synthetic routes to *N*-alkylcarbazole modified difluoroboron β-diketonate complexes **CnB** and **DCnB** (*n* = 2, 16) are shown in Scheme 1. Compounds **1-2**¹⁷ and

3-4^{12b} were prepared according to the reported procedures. The chlorination of **2a** and **2b** with SOCl₂ afforded **3a** and **3b**, respectively, without further purification. It should be noted that the excess SOCl₂ must be removed completely before use in the next step. After the enol anion was generated from cyclohexanone in presence of LDA, the α -acylation reaction underwent with **3a** to yield the ligand (9-ethyl-9*H*-carbazol-3-yl)(2-hydroxycyclohex-1-en-1-yl)methanone, which was complexed with boron trifluoride diethyl etherate directly without further purification to yield **C2B** in 55 % yield.^{12b} Similarly, **C16B** was synthesized from cyclohexanone, LDA and **3b**, followed by complexation with boron trifluoride diethyl etherate complex, in 62 % yield. Compound **4** was synthesized from cyclohexanone, LDA and acetyl chloride, followed by complexed with boron trifluoride diethyl etherate complex. Then, the Knoevenagel condensation reaction between compounds **4** and **1** in the presence of piperidine in anhydrous toluene gave **DC2B** and **DC16B** in a yield of 49 % and 42 %, respectively.¹⁹ The target molecules were characterized by ¹H NMR, ¹³C NMR, FT-IR, MALDI-TOF mass spectrometry and C, H, and N elemental analyses. The single crystal structure of **C2B** (CCDC 1810906) further confirmed the molecular structure. The bond length of (O)C1-C6 in aliphatic six-member ring was 1.383 Å, which was shorter than the bond length of C6-C7(O) (1.417 Å, see Fig. 4a), so we deduced that cyclohexenol was involved in **C2B**. In the FT-IR spectrum of **DC2B**, a vibration absorption peak at 965 cm⁻¹ was detected, meaning the *trans*-form of the vinyl groups. Similarly, the vinyl groups in **DC16B** also existed in the *trans*-form. The synthesized complexes are soluble in common solvents of THF, CH₂Cl₂ and toluene.

3.2. Photophysical properties in solutions

The UV-vis absorption and fluorescence emission spectra of **CnB** and **DCnB** in different solvents are shown in Fig. 1 and Fig. S1 (ESI[†]), and the corresponding photophysical data are summarized in Table S1 (ESI[†]). It was clear that **C2B** gave two absorption bands located at 329 nm and 400 nm in toluene, which were attributed to π - π^* transitions. With increasing the solvent polarity the absorption band at ca. 400 nm was red-shifted to a certain extent. Particularly, the fluorescence emission band of **C2B** gave significant red-shift with increasing the polarity of the solvents. For example, the emission was located at 451 nm in toluene and shifted to 539 nm in DMSO. Thus, the Stokes shifts increased with increasing the solvent polarities, and

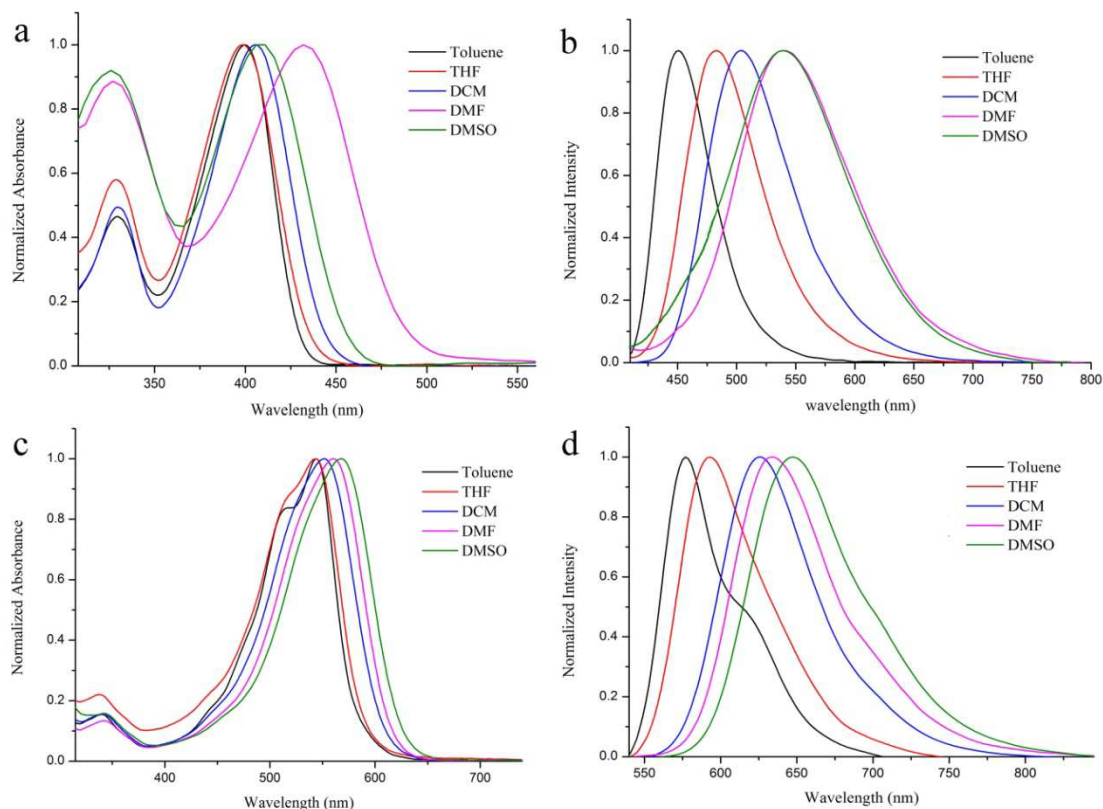


Figure 1. Normalized UV-vis absorption spectra of **C2B** (a) and **DC2B** (c), and fluorescent emission spectra of **C2B** (b, $\lambda_{\text{ex}} = 400$ nm) and **DC2B** (d, $\lambda_{\text{ex}} = 530$ nm) in different solvents (5.0×10^{-6} mol/L).

they were 2827 cm^{-1} and 5897 cm^{-1} in toluene and DMSO, respectively. Besides, **C2B** was highly emissive in THF with a fluorescence quantum yield (Φ_F) of 0.81 using 9,10-diphenylanthracene in benzene ($\Phi_F = 0.85$) as the standard, but Φ_F was only 0.07 in DMSO. The broadening and the red-shift of the emission band, the decreasing of Φ_F and the increasing Stokes shift ($2827\text{-}5897\text{ cm}^{-1}$) with increasing the solvent polarities illustrated the occurrence of ICT for **C2B** in polar solvents.²⁰ As depicted in Fig. S1a-b (ESI[†]), complex **C16B** gave similar UV-vis absorption and fluorescence emission spectra to **C2B** due to the same conjugated π -skeletons. When two *N*-alkylcarbazolyl-vinyl units were linked to the difluoroboron β -diketonate core, the absorption and emission bands were red-shifted compared with **CnB** on account of the enhanced degree of conjugation. As shown in Fig. 1c-d, **DC2B** gave a weak absorption at 339 nm and a strong absorption at 544 nm with a shoulder at 515 nm due to π - π^* transitions in toluene. With increasing the solvent polarities, the structured absorption bands were combined into one, which was red-shifted to 552 nm, 561 nm and 567 nm in DCM, DMF and DMSO, respectively. Moreover, the emission of **DC2B** appeared at 577 nm in toluene, and was red-shifted with increasing solvent polarity due to the strong interaction between excited state and solvent molecules.²¹ For example, the ICT emission of **DC2B** was red-shifted to 647 nm in DMSO. **DC16B** exhibited similar electronic spectra to those of **DC2B** in solutions.

3.3. Density function theoretical calculations

The Quantum chemical calculations were performed on **C2B** and **DC2B** by density functional theory (DFT) calculations at the B3LYP/6-31G level so as to reveal their electronic structures. As shown in Fig. 2, the HOMO and LUMO of **C2B** were mainly distributed in the carbazole unit (electron donor) and difluoroboron β -diketone moiety

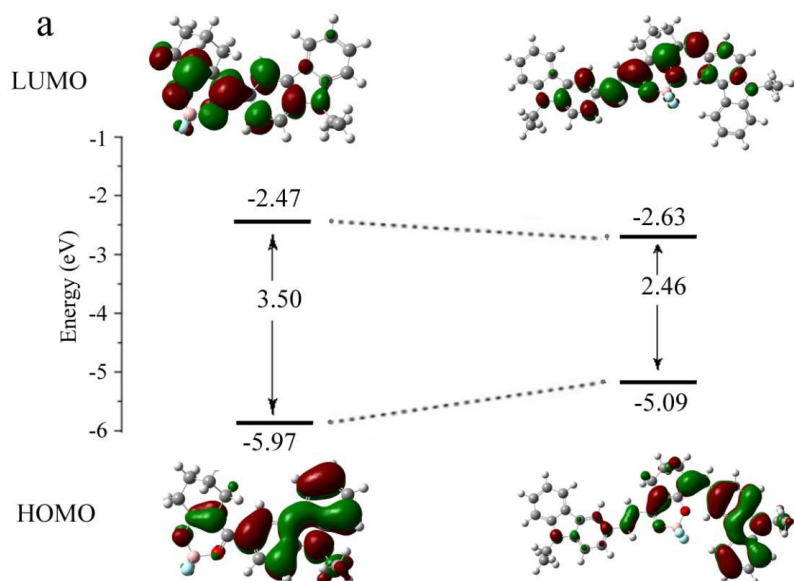


Figure 2. Energy levels and molecular orbital surfaces in the optimized ground-state structures.

(electron acceptor), respectively, suggesting a D- π -A type skeleton. **DC2B** is a typical D- π -A- π -D molecule, in which difluoroboron β -diketone acts as an electron withdrawing group, two carbazole groups are electron donors, and the vinyl moieties are involved as π -bridges. It was found that the HOMO of **DC2B** was located at the vinyl carbazole linked to cyclohexane and the LUMO was distributed in the acceptor and vinyl groups. Therefore, it was understandable that ICT emission was detected for **CnB** and **DCnB**. Meanwhile, the calculated LUMO energy level of **DC2B** was lower than **C2B**, but HOMO energy level of **DC2B** was higher than **C2B** because of the extended conjugation of **DC2B**. The low band gap for **DC2B** was in accordance with that its absorption and emission emerged in low-energy region compared with **C2B**.

On the other hand, the absorption wavelengths (λ_{abs}), oscillator strengths (f) and dominant excitation characters of **C2B** and **DC2B** were calculated with the TD-DFT/B3LYP/6-31G(d) functional. It was clear that their maximum absorption peaks

were derived from HOMO-LUMO transitions (Table S2). Because the frontier orbital plots of HOMOs and LUMOs for **C2B** and **DC2B** were mainly located at the donor and acceptor units, respectively, they possessed polar π -conjugated skeletons. It suggested that the ICT emission might be observed.

3.4. Mechanofluorochromic properties

As shown in Fig. 3a, **C2B** emitted strong green light in the as-synthesized sample, and the grinding led to the emitting color becoming yellowish green. The emission band was red-shifted to 519 nm in the ground powders compared with that at 504 nm in the as-synthesized sample. When the ground powders were fumed with CH_2Cl_2 vapor for

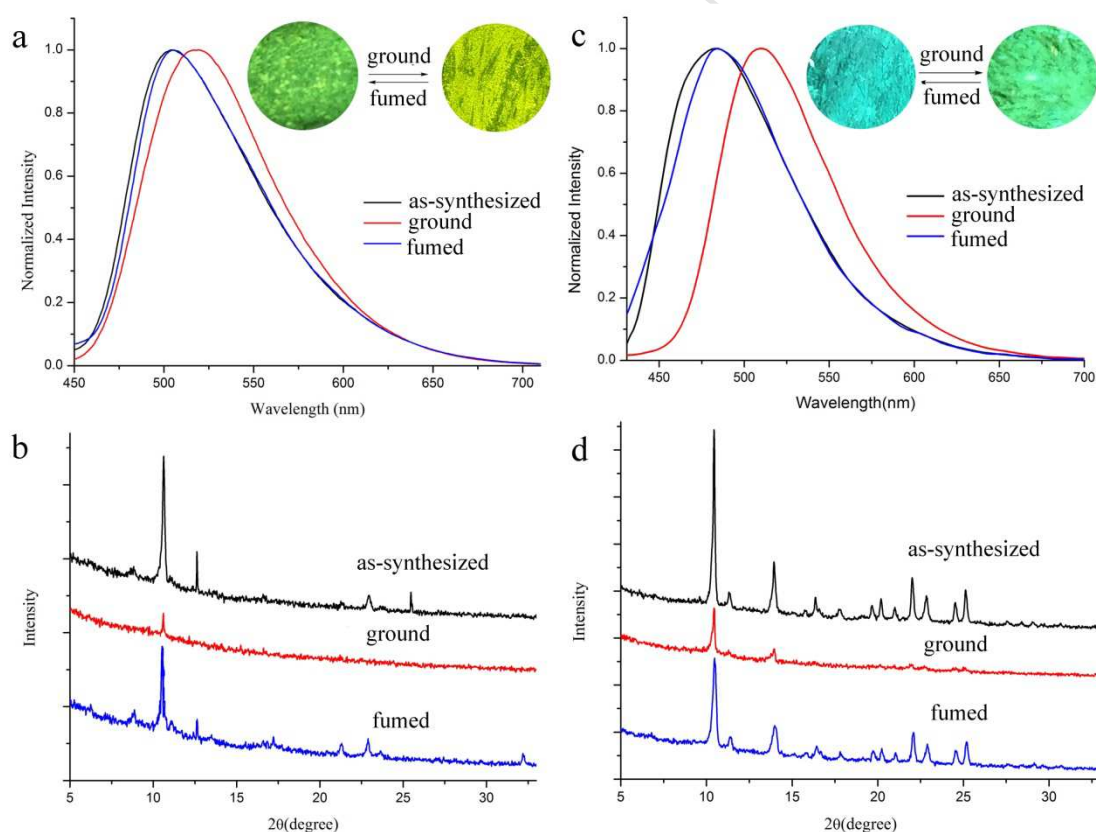


Figure 3. Normalized fluorescent emission spectra of **C2B** (a) and **C16B** (c) excited at 400 nm, and XRD patterns of **C2B** (b) and **C16B** (d) in different solid-state.

4 s or heated at 160 °C for 5 s, the emitting color could be recovered to green. Such changes could be repeated several times under grinding and solvent fuming/thermal treatment (Fig. S3a, ESI[†]), suggesting a fully reversible MFC processes. So as to reveal the MFC mechanism, the single crystal of **C2B** was obtained by slow evaporation from the solution in dioxane/cyclohexane. As shown in Fig. 4, we could find that the dihedral angle between carbazole and difluoroboron β -diketone moiety was 25.3° in single crystal of **C2B**. It was similar to the DFT calculations, which disclosed the dihedral angle of 28.1° between carbazole and difluoroboron β -diketone plane in **C2B** (Fig. S2, ESI[†]). It was clear that the molecules **C2B** were packed in a face-to-face mode, and the distance between two adjacent carbazole rings was 3.532 Å in the single crystal. Therefore, *J*-aggregates were involved in the single crystal of **C2B**, in which the hydrogen bonds of C–H...F and C–H... π were also formed. In detail, one of the fluorine atoms in the central molecule formed a hydrogen bond with hydrogen in cyclohexanone ring (2.571 Å), and the distance for C–H... π was 2.820 Å. The single crystal structure suggested that multiple intermolecular interactions would suppress the intramolecular rotation in the crystalline state, leading to strong luminescence of **C2B** in the solid-state. XRD patterns of **C2B** in different solid-state

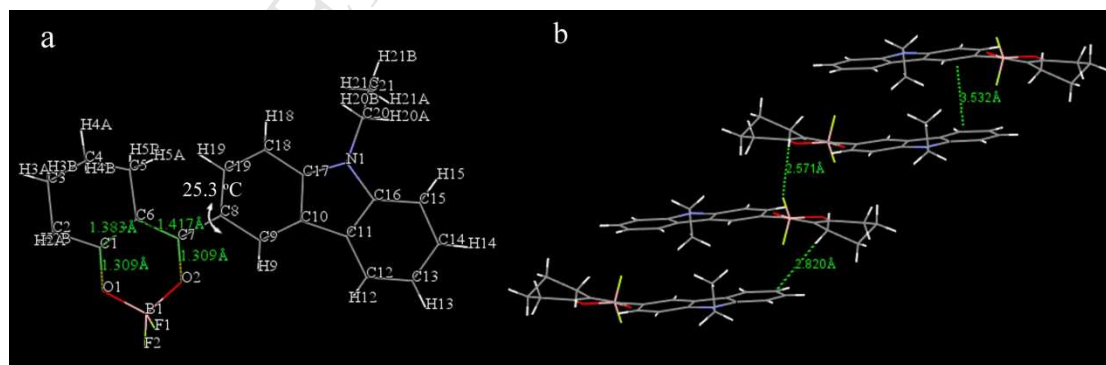


Figure 4. Molecular configuration (a) and single crystal structure of **C2B** (b).

were depicted in Fig. 3b. The as-synthesized sample of **C2B** gave several sharp and strong diffraction peaks, illustrating well-ordered crystalline structure. However, most of the diffraction peaks disappeared upon grinding, so we deemed that the ordered crystalline structures were transformed into an amorphous state under external mechanical force. After fuming with CH_2Cl_2 vapor, the diffraction peaks similar to those in the as-synthesized crystals emerged again. It meant that the reversible MFC process of **C2B** was originated from the transformation between crystalline and amorphous states. Furthermore, the UV-vis spectra of **C2B** in different solid-state were obtained in order to confirm the MFC mechanism. An absorption band at 454 nm was detected for **C2B** in the as-synthesized crystals and was blue-shifted to 424 nm in the ground powders (Fig. S5a, ESI[†]). Compared with the absorption at 400 nm of **C2B** in toluene, the red-shift of 54 nm was detected for the as-synthesized crystals, suggests the presence of *J*-aggregates in the crystals; a feature which is in accord with the result based on the single crystal structure. We deemed that parts of *J*-aggregates were destroyed in the ground powders, so the absorption of the ground powders was blue-shifted upon grinding. However, the emission of the ground powders of **C2B** emerged in low-energy region compared with the as-synthesized crystals, which might be due to greater planarity in ground powders might be better than that in as-synthesized crystals.

Although the conjugated skeletons of **C16B** and **C2B** were the same, **C16B** with long carbon chain in carbazole unit showed high-contrast MFC behavior compared with **C2B**. The as-synthesized crystals of **C16B** emitted blue fluorescence centered at 483 nm, and the emitting color of the ground powders was changed into bluish green with a maximal emission peak at 509 nm (Fig. 3c). Moreover, the reversible MFC processes could be also realized upon the treatment of grinding and fuming with

CH₂Cl₂ vapor for 3 s or heating at 80 °C for 2 s (Fig. S3b, ESI[†]). In addition, exposure of the ground powders of **C16B** under the vapor of THF or CHCl₃ for several seconds also induced the recovery of the emission to 483 nm (Fig. S4, ESI[†]). Although the emission of the ground powders was blue-shifted upon fumed with the vapor of C₂H₅OH or CH₃OH, it could not be fully recovered, which might be due to the poor solubility of **C16B** in C₂H₅OH or CH₃OH. Unfortunately, we could not gain the single crystal structure of **C16B**. The XRD patterns of **C16B** in different solid-state also illustrated that the transformation between crystalline and amorphous states was reasonable for the MFC behavior of **C16B** (Fig. 3d). Additionally, the absorption at ca. 421 nm of **C16B** in the as-synthesized crystals was observed in Fig. S5b (ESI[†]), and was ascribed to the electronic transition from the aggregated molecules (the absorption at 401 nm for **C16B** in toluene). When the as-synthesized crystals of **C16B** were ground, the absorption was blue-shifted to 416 nm. The changes of the electronic spectra of **C16B** during MFC processes were similar to **C2B**, e.g., the grinding lead to a red-shift of the emission and a blue-shift of the absorption. However, why do **C16B** and **C2B** exhibit different MFC properties? Firstly, the long alkyl chain in **C16B** might decrease the strength of π - π interactions in the as-synthesized crystals, so that its emission bands appeared at the high-energy region compared with **C2B**, for instance, the emission of **C16B** in crystals was located at 483 nm. Upon grinding, the disassembling of parts of π -aggregates and the improvement of the molecular planarity led to the red-shift of the emission of **C16B** to 509 nm. The high-contrast mechanofluorochromism of **C16B** was mainly originated from the high-lying excited state in the as-synthesized crystals.

When two terminal carbazole units were bridged by vinyl groups to link to difluoroboron β -diketonate cores, the large extended conjugation in **DCnB** induced

their solid emission to red-shift to the NIR region. As shown in Fig. 5a, **DC2B** emitted red light centered at 714 nm in the as-synthesized sample, which was blue-shifted to 703 nm (rose red) in the ground powders. The emitting color could be recovered to red when the ground powders were fumed with CH_2Cl_2 vapor for 8 s or heated at 240 °C for 5 s. The MFC behavior was reversible under the treatment of grinding/fuming or heating (Fig. S3c, ESI[†]). The XRD patterns of **DC2B** in different solid-state also illustrated that the transformation between the crystalline and amorphous states led to the reversible MFC properties (Fig. 5b). Meanwhile, **DC2B** gave two strong absorption bands located at ca. 546 nm and ca. 590 nm in the as-synthesized crystals. No obvious shift was detected for the two absorption bands after

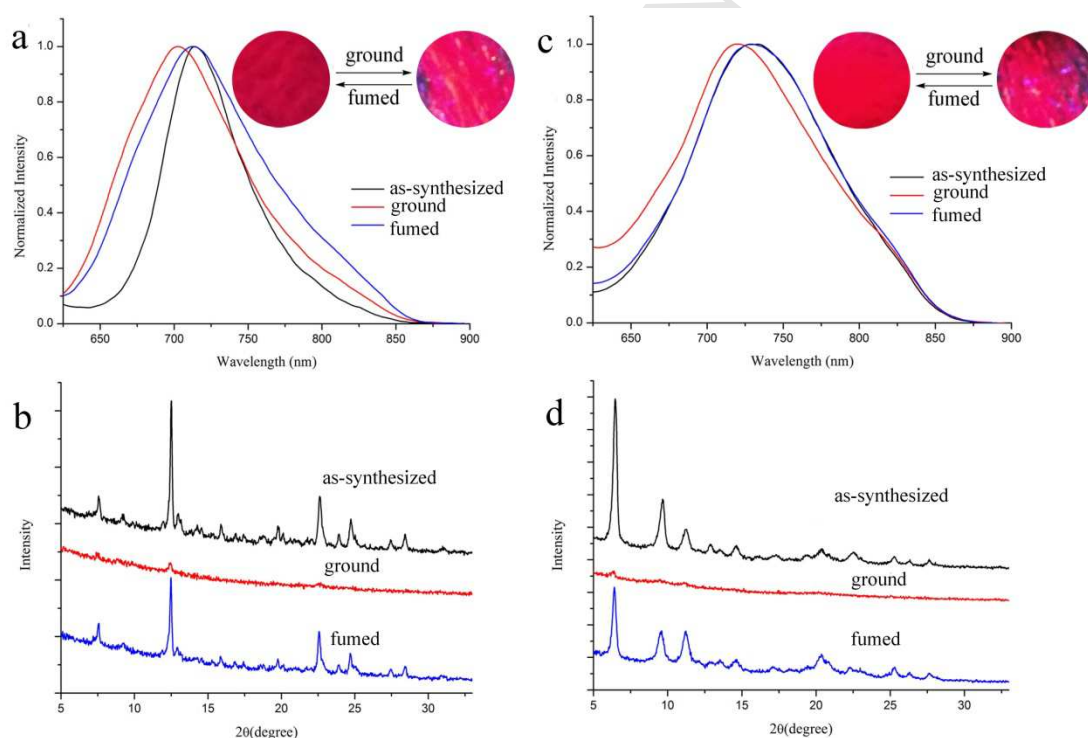


Figure 5. Normalized fluorescent emission spectra of **DC2B** (a) and **DC16B** (c) excited at 530 nm, and XRD pattern of **DC2B** (b) and **DC16B** (d) in different solid-state.

grinding the as-synthesized crystals of **DC2B**, except for the slight change of their relative intensities (Fig. S5c, ESI[†]). It is suggested that the isolated and aggregated molecules of **DC2B** were involved in both the as-synthesized crystals and the ground powders. The grinding might change the ratio of the contents of the isolated and aggregated molecules, leading to the change of the emitting colors. **DC16B** also exhibited reversible MFC properties (Fig. 5c-d and Fig. S3d, ESI[†]), and the emitting colors changed from red centered at 734 nm in as-synthesized crystals to rose red centred at 720 nm in ground powders. It should be noted that the emission peaks in as-synthesized and fumed samples of **DC16B** were fully overlapped, while the emission band for **DC2B** in the fumed sample was broader than in the as-synthesized crystals. We deemed that the long alkyl chain in **DC16B** might lead to looser molecular packing in crystals compared with **DC2B**, which would be beneficial for the recovery of luminescence. XRD patterns of **DC16B** in different solid-state further illustrated that the transformation between crystalline and amorphous states are responsible for MFC properties (Fig. 5d), which could be further proved by DSC curves of **DC16B** in different solid-state. As shown in Fig. S6 (ESI[†]), the ground powders of **DC16B** gave exothermic peaks at ca. 73.1 °C, except for the peaks corresponding to the melting points, meaning that the amorphous state was metastable.²³ It should be noted that the emission bands for **DC2B** and **DC16B** in the solid-state emerged in the range of 650-850 nm, such MFC materials with NIR emission was seldom reported.

4. Conclusions

In summary, new difluoroboron β -carbonyl cyclic ketonate complexes were synthesized, and they gave ICT emission in the solid-state. Interestingly, reversible MFC processes were detected for the four synthesized complexes. In detail, the

emission of **C2B** emerged at 504 nm in crystals, and was red-shifted to 519 nm upon grinding. The emitting color could be recovered to green from yellowish green upon fuming the ground powders with CH₂Cl₂ vapor. XRD patterns of **C2B** in different solid-state illustrated that the transformation between the crystalline and amorphous states were responsible for MFC behavior. However, **C16B** showed a red-shift of 26 nm upon the grinding as-synthesized crystals into ground powders, exhibiting relative high-contrast mechanofluorochromism compared with **C2B**. The reason might include the following points. The long alkyl chain in **C16B** would decrease the strength of π - π interactions in the as-synthesized crystals, so that its emission band appeared at high-energy region (483 nm). The disassembling of parts of π -aggregates as well as the improvement of the molecular planarity led to the red-shift of the emission of **C16B** to 509 nm upon grinding. Interestingly, in the case of **DC2B** and **DC16B**, in which two carbozole units were bridged by vinyl moieties to link to difluoroboron β -diketonate core, their emission appeared in the range of 650-850 nm in the solid-state, and gave red and rose-red luminescence in the as-synthesized crystals and in ground powders, respectively.

Acknowledgements

This work was financially supported by the National Natural Science Foundation of China (51773076 and 21503090) and the Open Project of State Key Laboratory of Supramolecular Structure and Materials (SKLSSM201813).

Supplementary data

Supplementary data related to this article can be found in the online version, at doi:

References

- [1] (a) Chi ZG, Zhang XQ, Xu BJ, Zhou X, Ma CP, Zhang Y, Liu S, Xu J. Recent advances in organic mechanofluorochromic materials. *Chem Soc Rev* 2012;41:3878–96.
- (b) Ma Z, Wang Z, Teng M, Xu Z, Jia X. Mechanically induced multicolor change of luminescent materials. *Chem Phys Chem* 2015;16:1811–28.
- (c) Zhang X, Chi Z, Zhang Y, Liu S, Xu J. Recent advances in mechanochromic luminescent metal complexes. *J Mater Chem C* 2013;1:3376–90.
- [2] (a) Davis DA, Hamilton A, Yang J, Cremer LD, Van Gough D, Potisek SL, Ong MT, Braun PV, Martinez TJ, White SR, Moore JS, Sottos NR. Force-induced activation of covalent bonds in mechanoresponsive polymeric materials. *Nature* 2009;459:68–72.
- (b) Meng X, Qi G, Zhang C, Wang K, Zou B, Ma Y. Visible mechanochromic responses of spiropyran in crystals *via* pressure-induced isomerization. *Chem Commun* 2015;51:9320–3;
- (c) Ma Z, Wang Z, Meng X, Ma Z, Xu Z, Ma Y, Jia X. A Mechanochromic single crystal: turning two color changes into a tricolored switch. *Angew Chem Int Ed* 2016;55:519–22.
- [3] (a) Chen Y, Spiering AJH, Karthikeyan S, Peters GWM, Meijer EW, Sijbesma RP. Mechanically induced chemiluminescence from polymers incorporating a 1,2-dioxetane unit in the main chain. *Nat Chem* 2012;4:559–62.
- (b) Mao Z, Yang Z, Mu Y, Zhang Y, Wang Y-F, Chi Z, Lo C-C, Liu S, Lien A, Xu J. Linearly tunable emission colors obtained from a fluorescent–phosphorescent dual-emission compound by mechanical stimuli. *Angew Chem Int Ed* 2015;54:6270–3.

- (c) Klukovich HM, Kouznetsova TB, Kean ZS, Lenhardt JM, Craig SL. A backbone lever-arm effect enhances polymer mechanochemistry. *Nat Chem* 2013;5:110–4.
- (d) Xu S, Liu T, Mu Y, Wang Y-F, Chi Z, Lo C-C, Liu S, Zhang Y, Lien A, Xu J. An organic molecule with asymmetric structure exhibiting aggregation-induced emission, delayed fluorescence, and mechanoluminescence. *Angew Chem Int Ed* 2015;54:874–8.
- (e) Tanioka M, Kamino S, Muranaka A, Ooyama Y, Ota H, Shirasaki Y, Horigome J, Ueda M, Uchiyama M, Sawada D, Enomoto S. Reversible near-infrared/blue mechanofluorochromism of aminobenzopyranoxanthene. *J Am Chem Soc* 2015;137:6436–9.
- (f) Zhang X, Chi Z, Li H, Xu B, Li X, Zhou W, Liu S, Zhang Y, Xu J. Piezofluorochromism of an aggregation-induced emission compound derived from tetraphenylethylene. *Chem Asian J* 2011;6:808–11.
- (g) Xie Z, Chen C, Xu S, Li J, Zhang Y, Liu S, Xu J, Chi Z. White-Light emission strategy of a single organic compound with aggregation-induced emission and delayed fluorescence properties. *Angew Chem Int Ed* 2015;54:7181–4.
- (h) Wang J, Mei J, Hu R, Sun JZ, Qin A, Tang BZ. Click synthesis, aggregation-induced emission, *E/Z* isomerization, self-organization, and multiple chromisms of pure stereoisomers of a tetraphenylethene-cored luminogen. *J Am Chem Soc* 2012;134:9956–66.
- (i) Matsunaga Y, Yang J-S. Multicolor fluorescence writing based on host–guest interactions and force-induced fluorescence-color memory. *Angew Chem Int Ed* 2015;54:7985–9.

(j) Sagara Y, Kato T. Stimuli-responsive luminescent liquid crystals: change of photoluminescent colors triggered by a shear-induced phase transition. *Angew Chem Int Ed* 2008;47:5175–8.

[4] (a) Dong YQ, Lam JWY, Tang BZ. Mechanochromic luminescence of aggregation-induced emission luminogens. *J Phys Chem Lett* 2015;6:3429–36.

(b) Yuan WZ, Tan Y, Gong Y, Lu P, Lam JWY, Shen XY, Feng C, Sung HHY, Lu Y, Williams ID, Sun JZ, Zhang Y, Tang BZ. Synergy between twisted conformation and effective intermolecular interactions: strategy for efficient mechanochromic luminogens with high contrast. *Adv Mater* 2013;25:2837–43.

(c) Dou C, Han L, Zhao S, Zhang H, Wang Y. Multi-stimuli-responsive fluorescence switching of a donor–acceptor π -conjugated compound. *J Phys Chem Lett* 2011;2:666–70.

(d) Sun H, Liu S, Lin W, Hang ZKY, Lv W, Huang X, Huo F, Yang H, Jenkins G, Zhao Q, Huang W, Smart responsive phosphorescent materials for data recording and security protection. *Nat Commun* 2014;5:3601–9.

(e) Li C, Tang X, Zhang L, Li C, Liu Z, Bo Z, Dong YQ, Tian Y-H, Dong Y, Tang BZ. Reversible luminescence switching of an organic solid: controllable on–off persistent room temperature phosphorescence and stimulated multiple fluorescence conversion. *Adv Opt Mater* 2015;3:1184–90.

(f) Woodall CH, Beavers CM, Christensen J, Hatcher LE, Intissar M, Parlett A, Teat SJ, Reber C, Raithby PR. Hingeless negative linear compression in the mechanochromic gold complex $[(C_6F_5Au)_2(\mu-1,4\text{-diisocyanobenzene})]$. *Angew Chem Int Ed* 2013;52:9691–4.

[5] (a) Lu QY, Li XF, Li J, Yang ZY, Xu BJ, Chi ZG, Xu JR, Zhang Y. Influence of cyano groups on the properties of piezofluorochromic aggregation-induced

emission enhancement compounds derived from tetraphenylvinyl-capped ethane.

J Mater Chem C 2015;3:1225-34.

(b) Xu BJ, He JJ, Mu YX, Zhu QZ, Wu SK, Wang YF, Zhang Y, Jin CJ, Lo CC, Chi ZG, Lien A, Liu SW, Xu JR. Very bright mechanoluminescence and remarkable mechanochromism using a tetraphenylethene derivative with aggregation-induced emission. Chem Sci 2015;6:3236-41.

(c) Xu BJ, Mu YX, Mao Z, Xie ZL, Wu HZ, Zhang Y, Jin CJ, Chi ZG, Liu SW, Xu JR, Wu Y-C, Lu P-Y, Lien A, Bryce MR. Achieving remarkable mechanochromism and white-light emission with thermally activated delayed fluorescence through the molecular heredity principle. Chem Sci 2016;7:2201-6.

(d) Wang C, Xu BJ, Li MS, Chi ZG, Xie YJ, Li QQ, Li Z. A stable tetraphenylethene derivative: aggregation-induced emission, different crystalline polymorphs, and totally different mechanoluminescence properties. Mater Horiz 2016;3:220-5.

(e) Xu BJ, Li WL, He JJ, Wu SK, Zhu QZ, Yang ZY, Wu Y-C, Zhang Y, Jin CJ, Lu P-Y, Chi ZG, Liu SW, Xu JR, Bryce MR. Achieving very bright mechanoluminescence from purely organic luminophores with aggregation-induced emission by crystal design. Chem Sci 2016;7:5307-12.

[6] (a) Liu T, Chien AD, Lu J, Zhang G, Fraser CL. Arene effects on difluoroboron β -diketonate mechanochromic luminescence. J Mater Chem 2011;21:8401-8.

(b) Zhang G, Singer JP, Kooi SE, Evans RE, Thomas EL, Fraser CL. Reversible solid-state mechanochromic fluorescence from a boron lipid dye. J Mater Chem 2011;21:8295-9.

- (c) Zhang G, Lu J, Sabat M, Fraser CL. Polymorphism and Reversible mechanochromic luminescence for solid-state difluoroboron azobenzene. *J Am Chem Soc* 2010;132:2160-2.
- (d) Nguyen ND, Zhang G, Lu J, Sherman AE, Fraser CL. Alkyl chain length effects on solid-state difluoroboron β -diketonate mechanochromic luminescence. *J Mater Chem* 2011;21:8409-15.
- (e) Morris WA, Butler T, Kolpaczynska M, Fraser CL. Stimuli responsive furan and thiophene substituted difluoroboron β -diketonate materials. *Mater Chem Front* 2017;1:158-66.
- (f) Morris WA, Sabat M, Butler T, DeRosa CA, Fraser CL. Modulating mechanochromic luminescence quenching of alkylated iodo difluoroboron dibenzoylmethane. *Materials J Phys Chem C* 2016;120:14289–300.
- [7] (a) Sagara Y, Yamane S, Mitani M, Weder C, Kato T. Mechanoresponsive luminescent molecular assemblies: an emerging class of materials. *Adv Mater* 2016;28:1073-95.
- (b) Pucci A, Bizzarri R, Ruggeri G. Polymer composites with smart optical properties. *Soft Matter* 2011;7:3689-700.
- (c) Sagara Y, Kato T. Mechanically induced luminescence changes in molecular assemblies. *Nat Chem* 2009;1:605-10.
- (d) Zhang Z, Wu Z, Sun J, Yao B, Zhang G, Xue P, Lu R. Mechanofluorochromic properties of β -iminoenolate boron complexes tuned by the electronic effects of terminal phenothiazine and phenothiazine-S,S-dioxide. *J Mater Chem C* 2015;3:4921-32.

- (e) Zhang Z, Xue P, Gong P, Zhang G, Peng J, Lu R. Mechanofluorochromic behaviors of β -iminoenolate boron complexes functionalized with carbazole. *J Mater Chem C* 2014;2:9543–51.
- (f) Zhang Z, Wu Z, Sun J, Xue P, Lu R. Multi-color solid-state emission of β -iminoenolate boron complexes tuned by methoxyl groups: aggregation-induced emission and mechanofluorochromism. *RSC Adv* 2016;6:43755–66.
- (g) Zhang G, Sun J, Xue P, Zhang Z, Gong P, Peng J, Lu R. Phenothiazine modified triphenylacrylonitrile derivatives: AIE and mechanochromism tuned by molecular conformation. *J Mater Chem C* 2015;3:2925–32.
- [8] (a) Shimizu M, Kaki R, Takeda Y, Hiyama T, Nagai N, Yamagishi H, Furutani H. 1,4-Bis(diarylamino)-2,5-bis(4-cyanophenylethenyl)benzenes: fluorophores exhibiting efficient red and near-Infrared emissions in solid state. *Angew Chem Int Ed* 2012;51:4095–9.
- (b) Han G, Kim D, Park Y, Bouffard J, Kim Y. Excimers beyond pyrene: a far-red optical proximity reporter and its application to the label-free detection of DNA. *Angew Chem Int Ed* 2015;54:3912–6.
- (c) Strobl M, Walcher A, Mayr T, Klimant I, Borisov SM. Trace ammonia sensors based on fluorescent near-infrared-emitting aza-BODIPY dyes. *Anal Chem* 2017;89:2859–65.
- (d) Wang J, Wu Q, Yu C, Wei Y, Mu X, Hao E, Jiao L. Aromatic ring fused BOPHYs as stable red fluorescent dyes. *J Org Chem* 2016;81:11316–23.
- [9] (a) Cogné-Laage E, Allemand J-F, Ruel O, Baudin J.-B, Croquette V, Desce MB, Jullien L. Diaroyl(methanato)boron difluoride compounds as medium-sensitive two-photon fluorescent probes. *Chem Eur J* 2004;10:1445–55.

(b) Ono K, Yoshikawa K, Tsuji Y, Yamaguchi H, Uozumi R, Tomura M, Taga K, Saito K. Synthesis and photoluminescence properties of BF₂ complexes with 1,3-diketone ligands. *Tetrahedron* 2007;63:9354-8.

(c) Xu S, Evans RE, Liu T, Zhang G, Demas JN, Trindle CO, Fraser CL. Aromatic difluoroboron β -diketonate complexes: effects of π -conjugation and media on optical properties. *Inorg Chem* 2013;52:3597-610.

[10] Galer P, Korosec RC, Vidmar M, Šket B. Crystal structures and emission properties of the BF₂ complex 1-Phenyl-3-(3,5-dimethoxyphenyl)-propane-1,3-dione: multiple chromisms, aggregation- or crystallization-induced emission, and the self-assembly effect. *J Am Chem Soc* 2014;136:7383-94.

[11] Sun X, Zhang X, Li X, Liu S, Zhang G. A mechanistic investigation of mechanochromic luminescent organoboron materials. *J Mater Chem* 2012;22:17332-9.

[12] (a) Liu MY, Zhai L, Sun JB, Xue PC, Gong P, Zhang ZQ, Lu R. Multi-color solid-state luminescence of difluoroboron β -diketonate complexes bearing carbazole with mechanofluorochromism and thermofluorochromism. *Dyes Pigm* 2016;128:271-8.

(b) Zhang F, Liu Q, Chen Y, Zhai L, Liu M, Sun J, Mi W, Sun M, Lu R. Mechanofluorochromism of D- π -A-type difluoroboron β -carbonyl cyclic ketonate complexes that contain a carbazole unit. *Asian J Org Chem* 2017;6:1659-66.

[13] (a) Cheng X, Li D, Zhang Z, Zhang H, Wang Y. Organoboron compounds with morphology-dependent NIR emissions and dual-channel fluorescent ON/OFF switching. *Org Lett* 2014;16:880-3.

(b) Xiao Q, Zheng J, Li M, Zhan SZ, Wang JH, Li D. Mechanically triggered fluorescence/phosphorescence switching in the excimers of planar trinuclear copper(I) pyrazolate complexes. *Inorg Chem* 2014;53:11604-15.

(c) Seki T, Tokodai N, Omagari S, Nakanishi T, Hasegawa Y, Iwasa T, Taketsugu T, Ito H. Luminescent mechanochromic 9-Anthryl Gold(I) isocyanide complex with an emission maximum at 900 nm after mechanical stimulation. *J Am Chem Soc* 2017;139:6514-7.

(d) Oda K, Hiroto S, Shinokubo H. NIR mechanochromic behaviours of a tetracyanoethylene-bridged hexa-perihexabenzocoronene dimer and trimer through dissociation of C-C bonds. *J Mater Chem C* 2017; 5:5310-5.

(e) Yang W, Liu C, Gao Q, Du J, Shen P, Liu Y, Yang C. A morphology and size-dependent on-off switchable NIR-emitting naphthothiazolium cyanine dye: AIE-active CIEE effect. *Opt Mater* 2017; 66:623-9.

[14] (a) Lu H, Zheng Y, Zhao X, Wang L, Ma S, Han X, Xu B, Tian W, Gao H. Highly efficient far red/near-infrared solid fluorophores: aggregation-induced emission, intramolecular charge transfer, twisted molecular conformation, and bioimaging applications. *Angew Chem Int Ed* 2016;55:155-9.

(b) Kowada T, Maeda H, Kikuchi K. BODIPY-based probes for the fluorescence imaging of biomolecules in living cells. *Chem Soc Rev* 2015;44:4953-72.

[15] Umezawa K, Citterio D, Suzuki K. New trends in near-infrared fluorophores for bioimaging. *Anal Sci* 2014;30:327-49.

[16] (a) Han Y, Cao H, Sun H, Wu Y, Shan G, Su Z, Hou X, Liao Y. Effect of alkyl chain length on piezochromic luminescence of iridium(III)-based phosphors adopting 2-phenyl-1H-benzimidazole type ligands. *J Mater Chem C* 2014;2:7648-55.

- (b) Bu L, Sun M, Zhang D, Liu W, Wang Y, Zheng M, Xue S, Yang W. Solid-state fluorescence properties and reversible piezochromic luminescence of aggregation-induced emission-active 9,10-bis[(9,9-dialkylfluorene-2-yl)vinyl]anthracenes. *J Mater Chem C* 2013;1:2028–35.
- (c) Xue S, Qiu X, Sun Q, Yang W. Alkyl length effects on solid-state fluorescence and mechanochromic behavior of small organic luminophores. *J Mater Chem C* 2016;4:1568–78.
- [17] Petrov RR, Knight L, Chen S-R, Wager-Miller J, McDaniel SW, Diaz F, Barth F, Pan HL, Mackie K, Cavasotto CN, Diaz P. Mastering tricyclic ring systems for desirable functional cannabinoid activity. *Eur J Med Chem* 2013;69:881-907.
- [18] Christoffers J, Kreidler B, Unger S, Frey W. Regioselective enamine formation from oxonia-borane-betaines and their application in asymmetric michael reactions. *Eur J Org Chem* 2003;2003:2845-53.
- [19] Zhai L, Liu M, Xue P, Sun J, Gong P, Zhang Z, Sun J, Lu R. Nanofibers generated from nonclassical organogelators based on difluoroboron β -diketonate complexes to detect aliphatic primary amine vapors. *J Mater Chem C* 2016;4:7939-47.
- [20] (a) Shen XY, Wang YJ, Zhao EG, Yuan WZ, Liu Y, Lu P, Qin A, Ma Y, Sun JZ, Tang BZ, Effects of substitution with donor–acceptor groups on the properties of tetraphenylethene trimer: aggregation-induced emission, solvatochromism, and mechanochromism. *J Phys Chem C* 2013;117:7334–47.
- (b) Zhang Y, Li D, Lia Y, Yu J. Solvatochromic AIE luminogens as supersensitive water detectors in organic solvents and highly efficient cyanide chemosensors in water. *Chem Sci* 2014;5:2710–6.

- [21] Zhang Z, Wu Z, Sun J, Yao B, Xue P, Lu R. β -Iminoenolate boron complex with terminal triphenylamine exhibiting polymorphism and mechanofluorochromism. *J Mater Chem C* 2016;4:2854-61.
- [22] (a) Molla MR, Gehrig D, Roy L, Kamm V, Paul A, Laquai F, Ghosh S, Self-assembly of carboxylic acid appended naphthalene diimide derivatives with tunable luminescent color and electrical conductivity. *Chem Eur J* 2014;20:760–71.
- (b) Hong GH, Qian C, Xue PC, Liu XL, Wang QQ, Gong P, Lu R. Linear oligocarbazole-based organogelators: synthesis and fluorescent probing of explosives. *Eur J Org Chem* 2014;2014:6155–62.
- [23] (a) Yang H, Ye KQ, Sun JB, Gong P, Lu R. Mechanofluorochromic behaviors of salicylaldehyde difluoroboron complexes. *Asian J Org Chem* 2017;6:199–206.
- (b) Sun J, Sun J, Mi W, Xue P, Zhao J, Zhai L, Lu R. Self-assembling and piezofluorochromic properties of *tert*-butylcarbazole-based Schiff bases and the difluoroboron complex. *Dyes Pigm*, 2017;136:633-40.

Highlights:

- New difluoroboron β -carbonyl cyclic ketonate complexes bearing *N*-alkylcarbazole were synthesized.
- The synthesized difluoroboron β -diketonate complexes showed reversible mechanofluorochromism.
- NIR dyes emitted red and rose red light during mechanofluorochromic processes.
- Dye **C16B** showed high-contrast mechanofluorochromism compared with dye **C2B**.

Highlights For

Mechanofluorochromism of NIR-emitting dyes based on difluoroboron β -carbonyl cyclic ketonate complexes

- New difluoroboron β -carbonyl cyclic ketonate complexes bearing *N*-alkylcarbazole were synthesized.
- The synthesized difluoroboron β -diketonate complexes showed reversible mechanofluorochromism.
- NIR dyes emitted red and rose red light during mechanofluorochromic processes.
- Dye **C16B** showed high-contrast mechanofluorochromism compared with dye **C2B**.